IEEE Access
Multidisciplinary ⋮ Rapid Review ⋮ Open Access Journal

Received September 2, 2020, accepted October 14, 2020, date of publication October 30, 2020, date of current version November 11, 2020.

Digital Object Identifier 10.1109/ACCESS.2020.3034833

Metasurface Matching Layers for Enhanced Electric Field Penetration Into the Human Body

SIMONE GENOVESI[1], (Senior Member, IEEE), IAN RICHARD BUTTERWORTH[2], (Member, IEEE), JOSÉ ENRIQUE CRUZ SERRALLÉS[2], (Graduate Student Member, IEEE), AND LUCA DANIEL[2], (Senior Member, IEEE)

[1]Dipartimento di Ingegneria dell'Informazione, University of Pisa, 56122 Pisa, Italy
[2]Research Laboratory of Electronics, Massachusetts Institute of Technology, Cambridge, MA 02139, USA

Corresponding author: Simone Genovesi (simone.genovesi@unipi.it)

This work was supported in part by the Project "Coil Design and Optimization for MRI of Medical Implants" through the MIT-UNIPI Program, and in part by the Italian Ministry of Education and Research (MIUR) in the framework of the CrossLab Project (Departments of Excellence).

ABSTRACT The use of electromagnetic fields applied to human tissues has proven to be beneficial in several applications, such as monitoring physiological parameters and delivering medical treatments. Often applications rely on targeted energy deposition into the tissue, or rely on wireless powering of implanted devices. In such cases, the system energy efficiency, the stability of the field, and ultimately the process safety could all benefit from minimizing the mismatch at the air-skin interface. In this article, the maximization of the electric field transmitted into the muscle tissue is initially addressed by optimizing a dielectric-only matching layer in terms of thickness and relative dielectric permittivity, and under realistic constraints on low-cost available materials. The propagation of the electromagnetic field inside a multilayered medium that represents the body is evaluated by using the wave-transmission chain matrix approach. Furthermore, an innovative solution, based on the application of a metasurface matching layer (MML), is proposed to significantly improve the performance of the matching, thus enhancing the electromagnetic fields reaching the targeted muscle tissue. A thorough assessment of the performance is carried out considering both the presence of an air gap, and the case of plane waves impinging at oblique incidence.

INDEX TERMS Biomedical applications, deep tissue coupling, metamaterials, plane wave excitation.

I. INTRODUCTION

Several studies have been devoted to the undesired interactions of electromagnetic fields and human [1]–[3] and to ways of preventing them [4]–[10]. On the contrary, in some biomedical applications there is instead often a need to maximize the desired penetration of electromagnetic fields into the body. This is beneficial in a broad range of applications, including more specifically: noninvasive diagnosis purposes [11], [12], medical treatments [13], [14], health and activity monitoring [15]–[17], biotelemetry [18], [19], and implantable medical devices [18], [20], [21].

The most adopted model for evaluating the propagation and absorption of electromagnetic fields in human tissue structures consists of a multilayered planar medium where each layer is considered homogeneous and with the proper electric and magnetic parameters that characterize a particular body region [22]–[24]. In this work, we consider a planar three-layer body model including a skin and a fat layer of thickness d_{skin} and d_{fat}, respectively (Fig. 1).

The muscle tissue layer is considered semi-infinite assuming that reflections from a fourth layer are negligible due to the overall attenuation experienced by the signal propagating in this layer. The assumed values of thickness and dielectric parameters (i.e. relative dielectric permittivity and loss tangent) for each tissue are reported in Table 1 and were selected based on large observational data collections [23]. Dispersion [25] is not considered, since the addressed applications do not exploit wideband frequency ranges.

Most of the solutions proposed in literature to ease the penetration of an electromagnetic field into the human body rely on the application of a medium that is designed to reduce

The associate editor coordinating the review of this manuscript and approving it for publication was Lei Zhao.

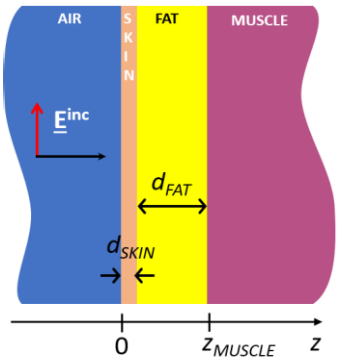

FIGURE 1. Considered starting scenario: a multilayered medium model of body tissues interrogated by an incident plane wave of $\underline{E}^{inc}$.

TABLE 1. Thickness and Dielectric Parameters of each Tissues Layer.

Tissue	ε_r	tgδ	Thickness (mm)
skin	39	0.32	2
fat	5.3	0.15	20
muscle	53.8	0.32	semi-infinite

the reflection at the air-skin interface. For instance, a single dielectric slab has been used in [15] and [26], whereas multiple layers have been adopted in [27]. In [28] the source is immersed in a lossless liquid whose properties are similar to the investigated tissue. A transmit-array lens in the middle of two water-bolus layers is proposed in [29]; water-bolus is also employed for matching purposes in [30] whereas a water-filled horn is exploited in [31].

The aim of this article is to investigate a matching layer (ML) configuration that is 1) thinner than solutions that require multilayer structures or liquid inclusions, but 2) does not sacrifice performance in terms of electromagnetic field penetration inside the muscle tissue, or 3) even improve penetration if a constraint on the thickness of such materials is enforced.

Our proposed solution consists of a metasurface applied to the air-skin interface that can provide effective matching, while exhibiting a low-profile structure. Examples of exploitations of metasurface properties are almost countless and cover a large area of applications [32]–[34]. Basically, such metasurfaces are formed by printing periodic metallic regions onto one or more dielectric slabs, and have recently been employed in applications such as distributed matching circuits for wearables [35], [36], low profile antennas [37], [38], and phased array antennas [39], [40].

In the first part of the study, we investigate the problem of a plane wave orthogonally impinging on the interface between air and skin, and we address the optimization of a dielectric layer by searching for a better impedance matching in order to improve the electric field penetration. We propose a solution based on the exploitation of a novel Metasurface Matching Layer (MML) and carry out a detailed study to demonstrate the remarkable improvement of the matching in terms of field penetrating into muscle tissue for a predefined maximum thickness. More in detail, the angular behavior for off-normal incident plane waves of different polarization is particularly relevant for modelling the interaction with the body and therefore it is studied to assess the suitability of the proposed MML. Finally, we consider a non-ideal configuration of the matching layer application to the skin (*i.e.* air gap) to verify the robustness of the MML approach.

This article is organized as follows. In Section II, we describe the theoretical approach and carry out the optimization of a dielectric-only matching layer. Section III focuses on estimating sensitivities to changes in body parameters. This can be beneficial when considering the application of the MML to different body parts or on different persons. Section IV considers the case of a non-ideal contact between the matching layer and the skin, by including an air gap in the model. Section V describes the design of the metasurface matching layer and analyses the electromagnetic field distribution inside the tissues. Finally, Section VI assesses the MML performance in the most challenging conditions (i.e. oblique incidence and air gap).

II. DIELECTRIC MATCHING LAYER OPTIMIZATION FOR IMPROVING ELECTRICAL FIELD PENETRATION

The scenario illustrated in Fig. 2 has been considered in order to assess the potentialities of a matching layer comprising a homogeneous layer of lossless dielectric. In order to search for a plausible solution for the aforementioned applicative scenarios, both in terms of thickness (d_{ML}) and relative dielectric permittivity of the dielectric matching layer (ε_{rML}), we constrained the set of considered values for d_{ML} to the range 1 mm – 20 mm, whereas ε_{rML} can assume values in the range 1 – 10. We consider a set of frequencies spanning between 1.0 GHz to 6.0 GHz, with a discrete step of 100 MHz (totalling 51 frequency points). The aim of the optimization is to maximize the electric field entering the muscle layer, namely at z = z_{miss}. The reflection and transmission calculations were performed by using the wave-transmission

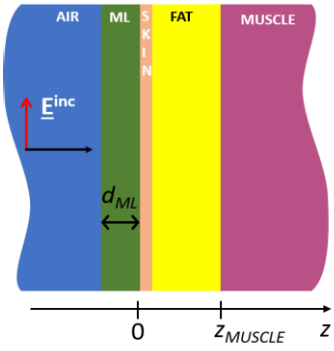

FIGURE 2. Exploitation of a dielectric matching layer on-skin for improving the incident electric field $\underline{E}^{inc}$ penetration into the muscle tissue.

chain matrix approach that models the electromagnetic field in each layer as the superposition of a forward and backward travelling wave [41].

This method allows us to easily evaluate the electromagnetic field in any point inside the tissue model. For instance, let us consider a forward-propagating TEM wave of amplitude c_1 impinging on a multilayered medium comprising n homogeneous layers of finite thickness l_i, each one with characteristic impedance ζ_i ($i = 1, \ldots, n$). A semi-infinite medium is implemented at the first and last interface with characteristic impedance ζ_0 and ζ_{n+1}, respectively (Fig. 3).

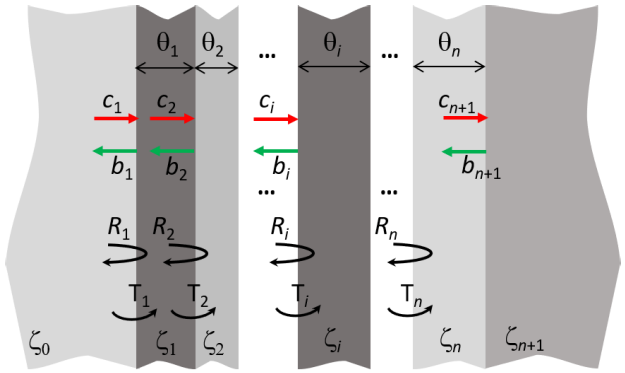

FIGURE 3. Multilayered medium analyzed as a cascade of *n* homogeneous dielectric layers.

By exploiting the boundary conditions at each interface, it is possible to evaluate the wave propagation in any point of the multilayered medium [41] and, in particular, between the impinging wave (c_1) and the wave transmitted in the last medium (c_{n+1}) by using the following relation:

$$\begin{pmatrix} c_1 \\ b_1 \end{pmatrix} = \prod_{i=1}^{n} \frac{1}{T_i} \begin{pmatrix} e^{j\theta_i} & R_i e^{-j\theta_i} \\ R_i e^{j\theta_i} & e^{-j\theta_i} \end{pmatrix} \begin{pmatrix} c_{n+1} \\ b_{n+1} \end{pmatrix} \tag{1}$$

where $\theta_i = k_i l_i$ is the electrical length of each layer calculated by using the physical length l_i and the propagation constant k_i inside that layer. The values of R_i and T_i, respectively the reflection and transmission coefficient looking into the i^{th} section, can be calculated as:

$$R_i = \frac{\zeta_{i+1} - \zeta_i}{\zeta_{i+1} + \zeta_i}; \quad T_i = \frac{2\zeta_{i+1}}{\zeta_{i+1} + \zeta_i}; \tag{2}$$

where ζ_i is the characteristic impedance of the i^{th} layer. Finally, c_i and b_i are the forward and backward propagating wave observed at the interface between the $(i\text{-}1)^{\text{th}}$ and i^{th} layer, respectively.

Let us first consider the case of a body comprising a skin layer of 2 mm and different fat layer thicknesses (1.6, 1.8 and 2.0 cm) allowing for representative variations in tissue characteristics across different parts of the body or on different subjects. The respective reflection and transmission coefficients are reported in Fig. 4. It is apparent that the electromagnetic field penetration is greater at lower frequencies and that a thicker fat layer generally causes a lower transmission level with a sole exception around 3 GHz.

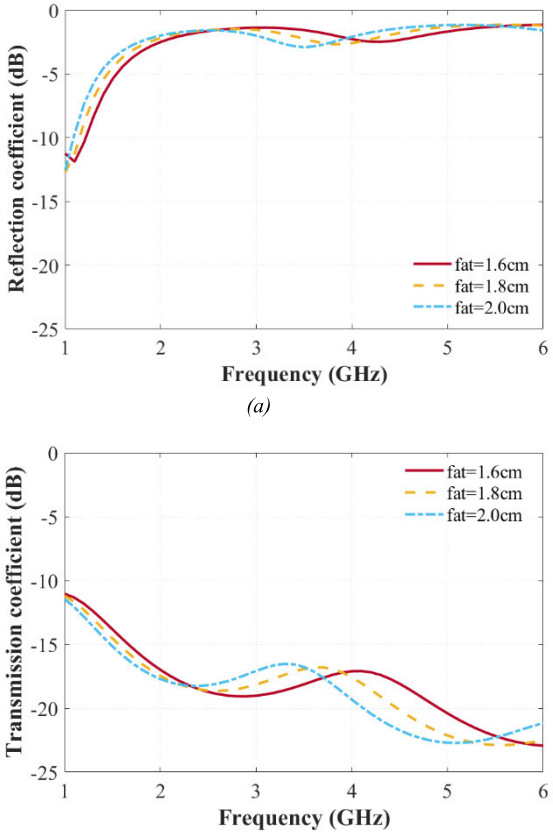

FIGURE 4. Reflection coefficient at z=0 and transmission coefficient at $z=z_{MUSCLE}$ as a function of frequency for different fat thicknesses (1.6 cm, 1.8 cm, 2.0 cm). The skin layer is 2mm-thick.

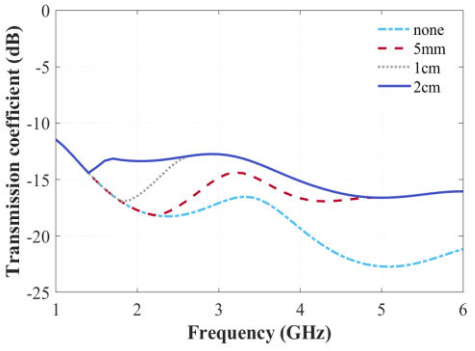

FIGURE 5. Highest transmission coefficient at $z=z_{MUSCLE}$ for different values of the maximum allowed thickness of the dielectric-only ML (5 mm, 1 cm and 2 cm) and maximum permittivity of 10. The skin layer and fat one are 2 mm- thick and 2cm-thick, respectively.

In order to improve the electromagnetic field penetration, we employ a lossless dielectric slab as a matching layer at the air-skin interface for a fat layer of 2 cm. The optimal values of matching layer permittivity and thickness are retrieved with an exhaustive search algorithm for each single frequency within the investigated range by considering a minimum thickness increment of 0.1 mm and a minimum step of 0.1 for the permittivity. Three different maximum values of the matching layer thickness are considered (5 mm, 1 cm

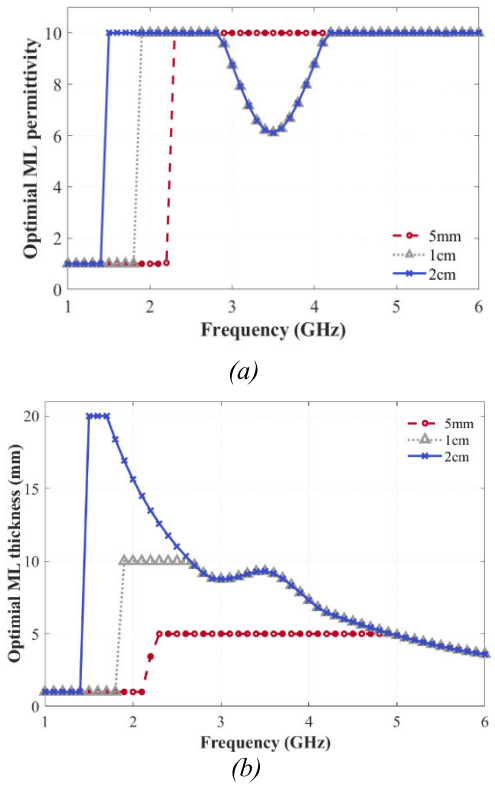

FIGURE 6. Optimal permittivity (a) and thickness (b) profile of the dielectric-only ML under the imposed constraints imposed to their maximum values. The skin and fat layers are 2mm-thick and 2cm-thick, respectively.

and 2 cm) whereas a maximum value of permittivity equal to 10 is allowed. If we consider such resolution in terms of thicknesses and dielectric permittivity, we obtain the results shown in Fig. 5. These assumptions can be hard to achieve in practice because bulk materials with the optimal permittivity values may not be available and because limitations in the thickness resolution can be reasonably hypothesized. However, it is informative to find the relative bound in terms of electromagnetic field penetration. The optimal thickness values and relative dielectric permittivity selected for minimizing the reflection coefficient (and thus maximizing the transmission into the muscle layer) are illustrated in Fig. 6. The thickness of the matching layer is the most influential parameter. In fact, for the case of thin dielectric layers (not thicker than 5 mm) there is no matching layer that can improve the performance for frequencies up to 2 GHz since the selected solution is just air. Between 2 GHz and up to 5 GHz the maximum thickness and maximum permittivity are the best options and some improvements can be obtained, as already illustrated in Fig. 5. Even better results are found at higher frequencies where the maximum permittivity is chosen but a smaller thickness is required. Thick matching layers can be beneficial to further increase the electrical field penetration within the interval 2-5 GHz and especially at lower frequencies where a 2-cm dielectric slab can considerably improve the transmission also between 1.2 GHz and 2 GHz (Fig. 5). It is pertinent to

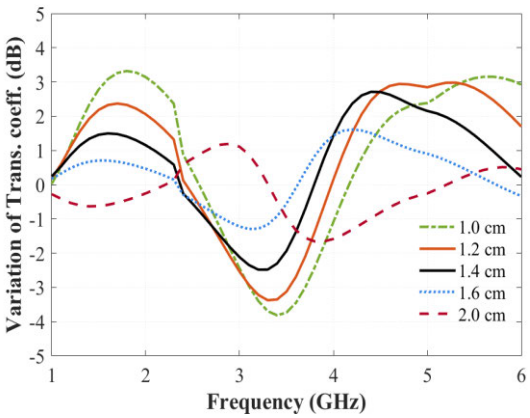

FIGURE 7. Variation of the transmission coefficient at $z=z_{MUSCLE}$ as a function of frequency for different fat thicknesses when the matching layer has been optimized for a fat thickness of 1.8 cm. The skin layer is 2 mm-thick whereas the maximum allowed thickness for the matching layer is 5 mm.

highlight that a 2 cm-thick dielectric slab of high permittivity would likely be a cumbersome and unpractical solution in several practical scenarios and therefore a reduction in the overall dimension of the matching layer must be pursued.

III. EFFECT OF BODY PARAMETERS

Another important consideration in the design of a matching layer is related to the change in performance when different tissue values are considered as a result of variation across person and location on body (*e.g.* fat thickness). It is therefore useful to estimate the impact of these potential changes in the level of transmitted electric field, in order to assess the limits of an optimal matching layer configuration when subjected to variations. To have a robust matching layer solution it is essential to verify that the performance is stable or at least a gentle deterioration with respect to the optimal scenario of reference. To investigate this stability, first a matching layer has been optimized for a representative tissue model comprising a fat layer of thickness 1.8 cm, and subsequently tested against tissue models comprising of fat thicknesses varying between 1.0 cm and 2.0 cm (at 0.2 cm intervals). Two maximum thicknesses of the matching layer were considered, namely 5 mm (Fig. 7) and 2 cm (Fig. 8).

In both cases, when the matching layer that was optimized for a fat layer of 1.8 cm was applied to a body exhibiting a variation in the order of $\pm 10\%$ (i.*e.* 1.6 cm and 2.0 cm), there is a variation of the transmission coefficient at the fat-muscle interface on the order of $\pm$1dB with a slightly higher difference in the case of the thinner matching layer. Modelling of thickness variations outside of this 10% resulted in erratic variations, changing considerably ($> \pm$3dB) as a function of the chosen working frequency. It is important to emphasize that the optimization here of matching layer thickness and permittivity parameters (d_{ML}, ε_{rML}) was conducted for a singular desired frequency; therefore, optimization of parameters cannot be assumed for even adjacent frequencies (as illustrated in Fig. 6). The variations of almost 4 dB

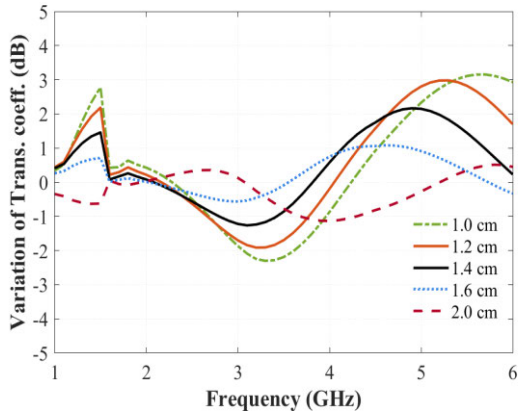

FIGURE 8. Variation of the transmission coefficient at $z=z_{MUSCLE}$ as a function of frequency for different fat thicknesses when the matching layer has been optimized for a fat thickness of 1.8 cm. The skin layer is 2 mm-thick whereas the maximum allowed thickness for the matching layer is 2.0 cm.

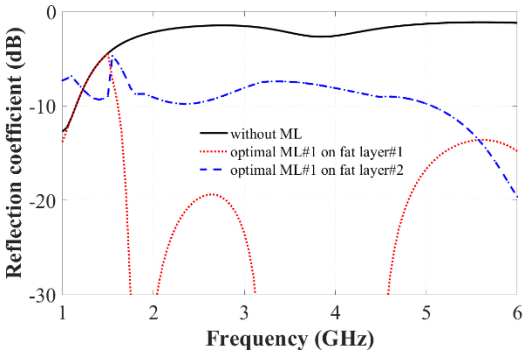

FIGURE 9. Example of the effect of applying a matching layer optimized for a fat layer of 1.8 cm (layer#1) to a body with a fat layer of different thickness (layer#2). In the reported case laye#2 has thickness 1.0 cm.

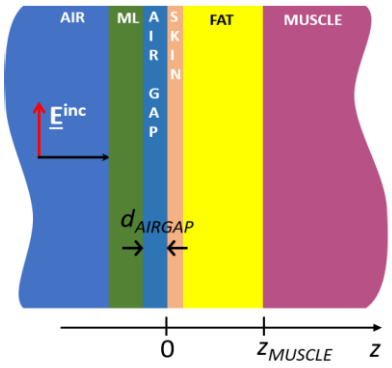

FIGURE 10. Non-contact case: an air gap is present between the ML and the body.

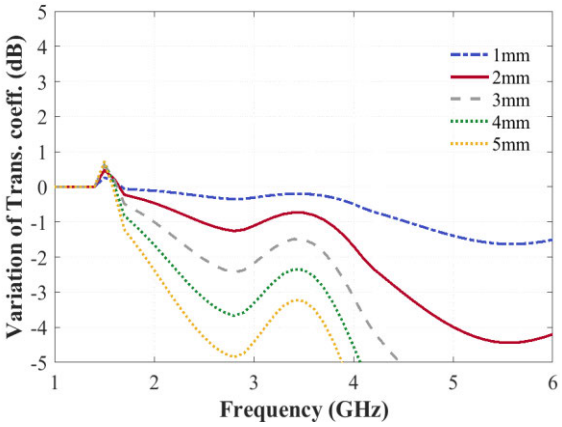

FIGURE 11. Variation of the transmission coefficient at $z=z_{MUSCLE}$ as a function of frequency for different air gap thicknesses for a matching layer optimized for a fat thickness of 1.8 cm and without the air gap. The skin layer is 2mm-thick whereas the maximum allowed thickness for the matching layer is 2 cm.

that were observed for the case of thinner matching layers (Fig. 7) suggest that a thicker layer (Fig. 8) provides more stable performance. The positive variations of the transmission coefficient are simply due to a lower level of absorption loss determined by considering fat layers thinner than 1.8 cm. As a final note, the abrupt change that is particularly visible in Fig.8 can be explained referring to Fig.9, where the reflection coefficient is reported for three different scenarios. The black line represents the reflection coefficient related to a body with a 1.8-cm layer of fat and without any matching layer. The dotted red line is the reflection coefficient for the same body when the optimal matching layer is applied. It is apparent that the matching layer starts to be effective starting from around 1.5 GHz, due to the restrictions imposed in terms of thickness and permittivity of the allowed dielectrics for the matching layer. Before this frequency, the best choice is to not adopt any matching layer and therefore the reflection level does not decrease. As a comparison, the reflection coefficient of the optimized matching layer is tested on a different bidy, where the thickness of the fat layer is 1.0 cm. Although the overall performance are not optimal as expected, it is evident that even in this case where the fat layer is changed the effect of the matching layer is still beneficial.

IV. EFFECT OF AN AIR GAP

Although some applications can reasonably assume that it is possible to apply the matching layer directly in contact with the skin, in other cases, such as a wearable device, this is not always true. It is therefore necessary to include an air gap of thickness d_{AIRGAP} in the model (Fig. 10).

The effect of this additional layer was considered by looking at the variation of the transmission coefficient at the fat - muscle interface when an air gap of increasing thickness is placed between the matching layer, which was optimized in absence of the air gap, and the skin (Fig. 11). It is clear that the presence of an air gap can be tolerated if the size of said air gap is up to 1 mm, with a variation of < 2dB across almost the full 1-6 GHz frequency range, and for a 2 mm air gap, similar magnitude variations between 1-4 GHz. However, for thicker air gaps, although air gap thickness is a fraction of the considered wavelength, the performance rapidly deteriorates even at low frequencies.

If the presence of the air gap is included in the model during the optimization stage, the achieved results seem more robust. In fact, if the matching layer is optimized by considering an air gap of thickness $d_{AIRGAP} = 1$ mm and then the air gap is changed (Fig. 12), the variation of the transmission

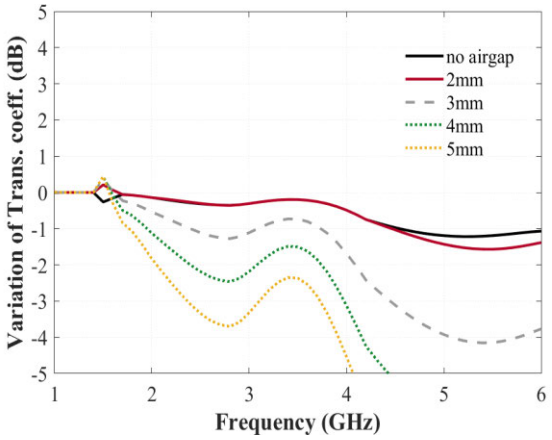

FIGURE 12. Variation of the transmission coefficient at $z = z_{MUSCLE}$ as a function of frequency for different air gap thicknesses for a matching layer optimized for a fat thickness of 1.8 cm and with $d_{AIRGAP} = 1$ mm. The skin layer is 2mm-thick whereas the maximum allowed thickness for the matching layer is 2 cm.

coefficient is acceptable both when no air gap is present as well as when the air gap is increased to 2 mm.

A further increase of the spacing between the matching layer and the skin may be still considered tolerable up to 4 GHz but for higher frequencies or thicker air gaps the transmission suffers a significant degradation (more than - 1 dB). Moreover, the average transmission coefficient obtained by optimizing the case of a 1mm-thick air gap was identical to the one achieved by optimizing with no air gap (- 14.49 dB instead of - 14.47 dB).

V. METASURFACE MATCHING LAYER FOR PLANE WAVE INCIDENCE

We observed in our previous investigations that a matching layer thickness greater than 5 mm is necessary to achieve a good level of matching between the body and the impinging electromagnetic field, with required optimal thicknesses of more than 1 cm (Fig. 6). In view of reducing the thickness of the matching layer to ease its application and wearability, a novel approach based on the use of a metamaterial was investigated. The aim was to design a suitable periodic surface, a MML, to be applied on the skin for adapting the body impedance to the free space one. The first step was to determine the impedance of the body at the interface air-skin. By using the multilayered medium model illustrated in Fig. 1 the real and imaginary part of the impedance offered by the body was evaluated for different values of fat thicknesses (Fig. 13). It is apparent that the body exhibits a capacitive impedance in the range between 1 GHz and 3 GHz and after that has an inductive behavior. The real part exceeds 50 Ohm below 2 GHz and is generally lower elsewhere.

In order to prove the effectiveness of using a metasurface matching layer in achieving better electromagnetic field penetration in the muscle tissue, a test case frequency $f_0 = 1.5$ GHz was considered as the working frequency [42], [43]. This frequency lies within the range that requires the thickest dielectric-only matching layers (Fig. 6) with an impedance

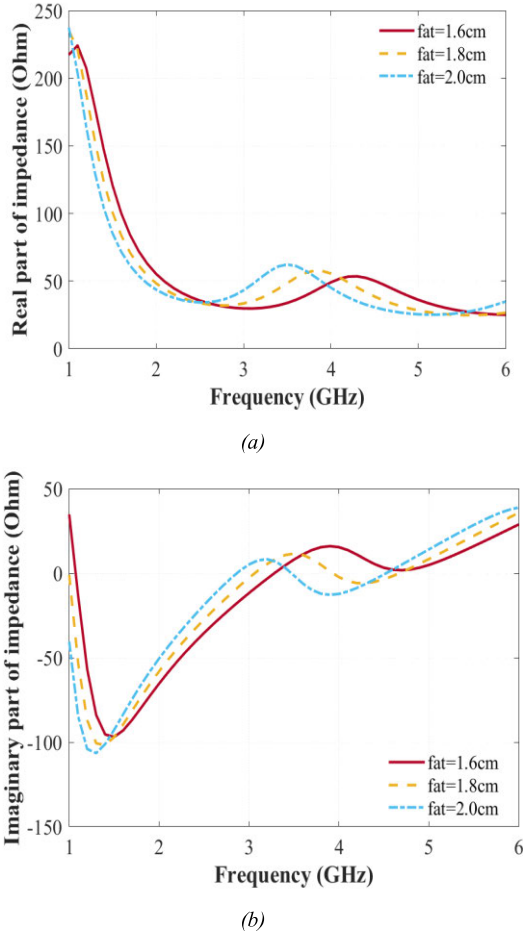

FIGURE 13. Impedance of multilayered medium model for the body: real (a) and imaginary part (b).

having a strong capacitive behavior (Fig. 13) and therefore can be considered a challenging task. The aim of the design procedure exploiting the metasurface features was twofold and consisted of reaching a comparable level of matching than the one obtained with a dielectric-only matching layer while obtaining this result with a thinner structure in tandem. In particular, a dielectric slab of 3 mm with permittivity equal to 10 was considered as the hosting layer for the periodic structures (Fig. 14).

The degrees of freedom offered by this design are geometric, covering the size and shape of the inclusions, and the lattice in which they are placed [44]. Since the body has a significant capacitive impedance behavior, the metasurface matching layer must offer an inductive loading effect. Therefore, a square wire mesh of width s is repeated along x and y direction with a period T printed on the dielectric slab is considered as a preliminary promising candidate [45] to be properly tailored to achieve the desired matching at frequency f_0. The structure reported in Fig. 14 was analyzed by using a full-wave numerical method based on the Periodic Method of Moments (PMoM) [44]. To better highlight the change in the frequency response of the body with the metasurface matching layer applied, the reflection coefficient for some

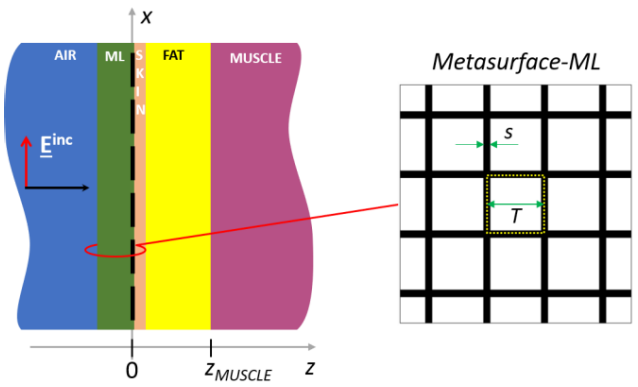

FIGURE 14. .Metasurface matching layer application for improving the incident electric field $\underline{E}^{inc}$ penetration into the muscle tissue.

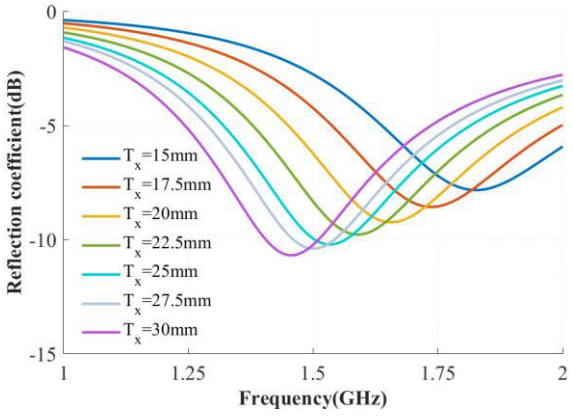

FIGURE 15. Reflection coefficient for different values of the periodicity T of the metasurface matching layer comprising a square wire mesh. The thickness of the dielectric slab hosting the periodic surface is equal to 3 mm and its permittivity is 10.

values of the lattice periodicity T was plotted (Fig. 15). The width s was varied too, since it is equal to $T/16$ due to the discretization scheme imposed by the PMoM. The results are illustrated as a function of frequency for values of T within the range [15 mm-30 mm].

The reported results suggest that the best choice for minimizing the reflection coefficient (and thus maximizing the electric field penetration in the body) takes place for a periodicity $T = 27.5$ mm. In order to verify this result, a full-wave simulation was carried out using ANSYS Electromagnetic Suite v18 [46]. In particular, the transmission of the electromagnetic field using the metasurface matching layer with respect to a dielectric slab of same thickness and the best dielectric-only matching layer were compared. Moreover, the electric field distribution in the muscle tissue was evaluated as well to assess the homogeneity of the electromagnetic power distribution since this could be important for dimensioning an efficient link with in-body devices that is also robust with respect to their position. A cross section (zx-plane) of the multilayered tissue model exposed to the impinging radiation is reported Fig. 16 for an incident power of 1 W. The strong interaction among the metasurface matching layer and the skin where the electric field amplitude is

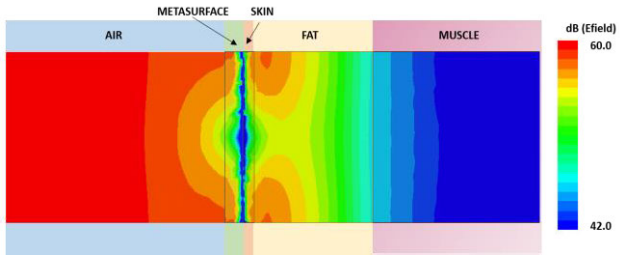

FIGURE 16. Electric field magnitude at frequency f_0 inside the body. The section is on zx-plane and the impinging electric field is polarized along x. The logarithmic color map scale is reported in the inset.

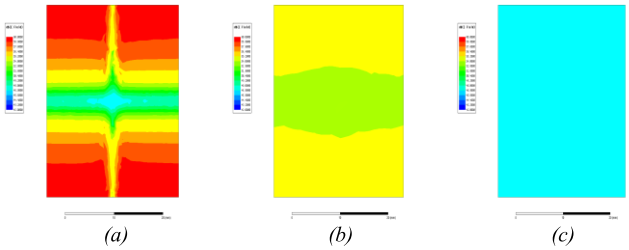

FIGURE 17. Distribution of the electric field magnitude on different transverse planes: in the middle of the skin layer(a), in the middle of fat layer (b), in the muscle layer at 1 mm from the fat-muscle interface (c). The logarithmic color map scale is the same reported in Fig.16.

not homogeneous is well visible. However, the electric field distribution is regular in the fat layer and even more at the interface between fat and muscle as clearly visible if we look at the square transverse sections of side T that are reported in Fig. 17. At a distance of 1 mm in the muscle tissue the electric field distribution is almost constant throughout the entire the layer.

The electrical field magnitude that reaches the fat-muscle interface was evaluated and compared for three different configurations of the matching layer (Fig. 18), namely the MML case, the optimal dielectric-only one (*2cm Diel-only ML*) and finally by considering a dielectric slab of the same thickness of the metasurface one (*3mm Diel-only ML)*. In all the three cases, the relative dielectric permittivity of the employed material was equal to 10. The electrical field magnitude along the y-direction was plotted in the middle of the skin and fat layers and at 1 mm from the fat-muscle interface.

First of all, it is possible to appreciate the regularity of the electric field distribution in the fat and muscle layer right after the interface. The non-perfect symmetry of the field is due to non-exact symmetry of the mesh which determines small numerical discrepancies. Moreover, it can be stated that the performance of the metasurface matching layer is equivalent to the one achieved by the optimal dielectric-only matching layer. However, it is worthwhile to highlight that the same level of electric field is obtained in the muscle by using a metasurface matching layer exhibiting an 85% thickness reduction with respect to the dielectric-only optimal matching layer. Finally, if the comparison is carried out with a dielectric matching layer of the same thickness (*i.e.* 3 mm), the result is an electric field that is more than 2 dB higher if the metasurface matching layer is applied.

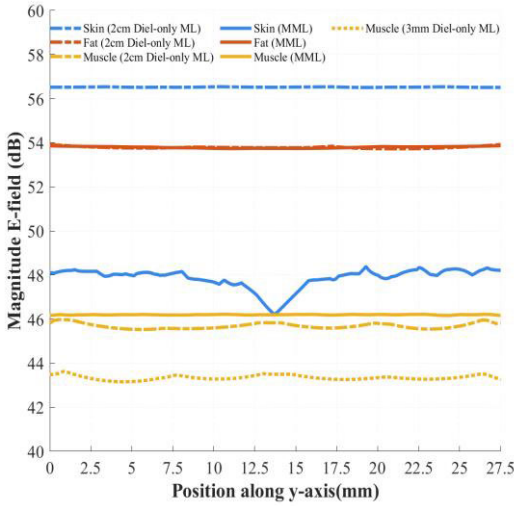

FIGURE 18. Electric field amplitude distribution along y-direction inside different tissues: in the middle of skin and fat layer and at 1 mm from the fat-muscle interface.

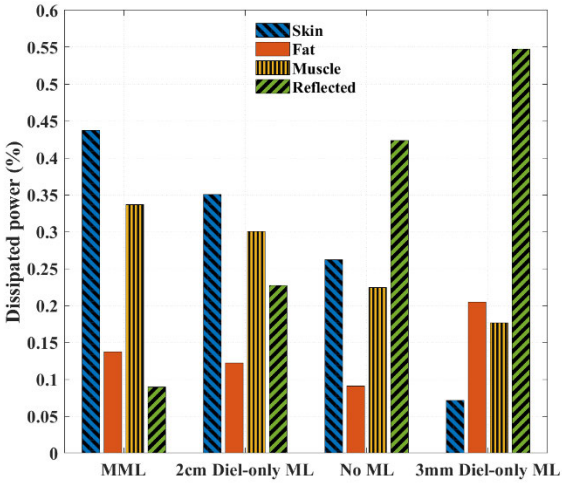

FIGURE 19. Electric field amplitude distribution along y-direction inside different tissues: in the middle of skin and fat layer and at 1 mm from the fat-muscle interface.

This assessment proves that a significant reduction of the matching layer thickness can be achieved if a metasurface matching layer is employed, thus providing opportunities for lower-profile applicator embodiments allowing greater control of ergonomic design factors. The technology necessary to manufacture such metasurfaces could be the same technology that is used for standard printed electronics [35], [47], resulting in cost-efficiency. If the distance between source antenna and skin is a strong design constraint, for the same thickness, a metasurface matching layer can provide a considerable increase in power efficiency by offering superior performance compared to that of a standard dielectric substrate.

A comprehensive view of the performance provided by the different solutions is illustrated in Fig. 19 where the levels of dissipated power inside the body layers (*i.e.* skin, fat, muscle), as well as the reflected one, are compared. It is interesting to notice that the MML solution allows the higher level of electric field in the muscle tissue, where almost 35% of the incident power is dissipated, and determines the lower level of reflection, that is less than 10%. The 2cm Diel-only ML performed slightly worse in the muscle tissue (30% of dissipated power) whereas the 3mm Diel-only ML solution suffered from a strong reflection (around 55% of the incident power). The absence of any matching layer determines a high reflection (around 45%) and a modest dissipated power in the muscle (less than 25%).

VI. ANALYSIS FOR OBLIQUE INCIDENCE AND EFFECT OF AN AIR GAP ON METASURFACE MATCHING LAYER

The effect of oblique incidence was addressed since it provides useful information on how the metasurface is going to interact with a spectrum of incident plane waves. For off-normal incidence, the polarization of the electric field with respect to the plane of incidence (xy-plane in Fig.20) can be TE (*i.e.* E-field parallel to y-axis) or TM (*i.e.* E-field on xz-plane) [48].

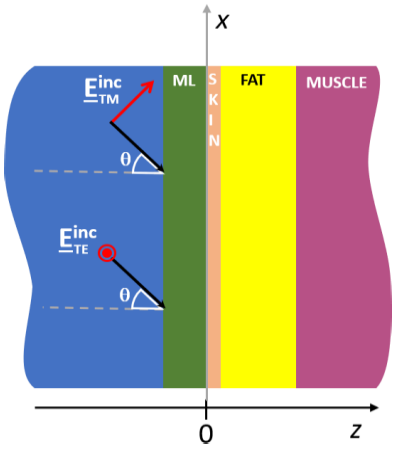

FIGURE 20. Oblique incidence of a plane wave: E-field parallel to the *xy*-plane of incidence (*i.e.* TM case) and orthogonal to it (*i.e.* TE case).

The reflection at the interface can significantly vary in the two cases since in the former, the E-field is always parallel to the plane of incidence whereas in the latter, there is a not negligible E-field component orthogonal to the interface. The power dissipated in the muscle tissue for the TE case at oblique incidences ($\theta = 30°, 45°, 60°$) is compared to the normal incidence case in Fig. 21 for the 2 cm and 3 mm dielectric-only matching layers and the MML. It is shown that the MML provides the best results since it offers stable results in terms of dissipated power, which is around 35% of the incident one, and it is slightly higher than the thickest dielectric matching layer, with the only exception of $\theta = 60°$.

An even more favorable trend for the MML is visible in Fig. 22 where it outperforms the thickest matching layer by, at least, 5% of the power provided to the muscle tissue and by more than 15% of the same-thickness structure.

These results assess the overall better performance of the metasurface matching layer for both polarizations with respect to the dielectric-only solutions. As it can be seen, the metasurface-ML exhibits a gentle decrease of performance

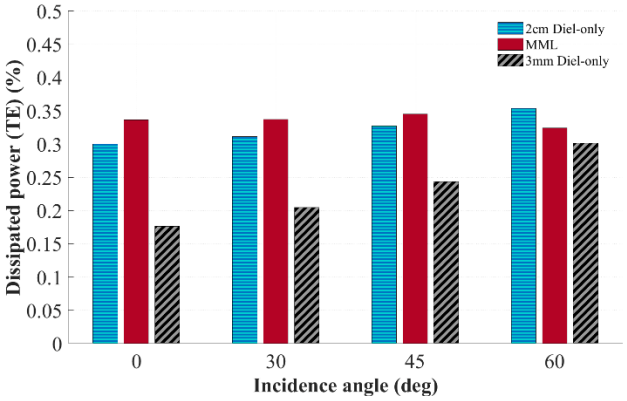

FIGURE 21. Dissipated power in the muscle tissue for a TE incident plane wave at oblique incidence (θ = [30 deg, 45°deg, 60°deg]).

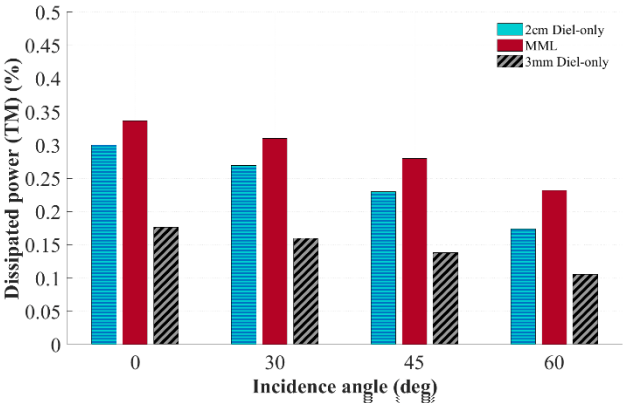

FIGURE 22. Dissipated power in the muscle tissue for a TM incident plane wave at oblique incidence (θ = [30 deg, 45°deg, 60°deg]).

with respect to normal incidence plane waves, but the offered off-normal response remains a better option than the one of a dielectric-only matching layer.

The introduction of an air gap alters the original boundary conditions assumed during the design process and therefore this kind of analysis verifies the robustness of the solution. A desirable feature that a MML applied to the human body should exhibit is the stability or gentle degradation of its performance in non-ideal situations, such as in the presence of an air gap, as illustrated in Fig. 10.

This analysis was performed both for normal and oblique incidences. More in detail, an air gap between the MML and the skin was considered to assess the overall performance improvement with respect to the two dielectric-only matching layers considered so far (*i.e.* 2 cm and 3 mm). The power dissipated in the muscle tissue is still considered the figure of merit for ranking the three candidate solutions. The addressed cases include three different air gap thicknesses (i.e. 1 mm, 2 mm and 3 mm). The normal incidence case is illustrated in Fig. 23 where it is apparent that MML performance is comparable with those of the much thicker dielectric-only matching layer and better than the ones of the matching layer of same thickness.

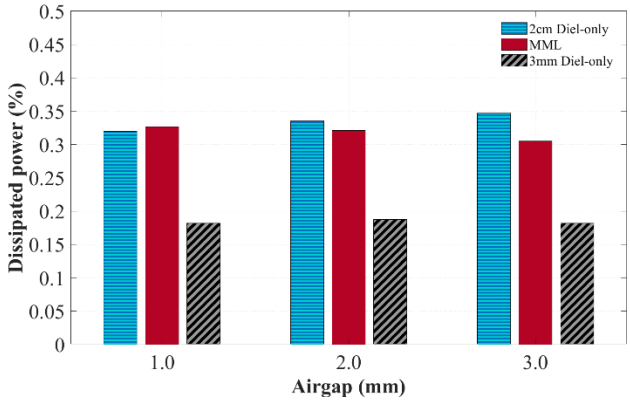

FIGURE 23. Dissipated power in the muscle tissue for the three investigated matching layer configuration for different thickness of the air gap.

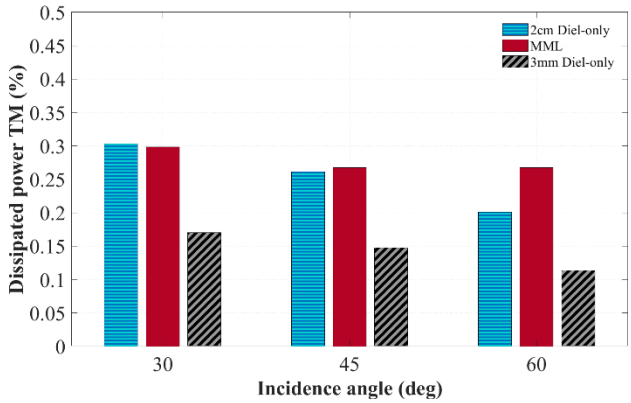

FIGURE 24. Dissipated power in the muscle tissue for a TM plane wave impinging at three different incidence angles. The considered air gap thickness is 2 mm.

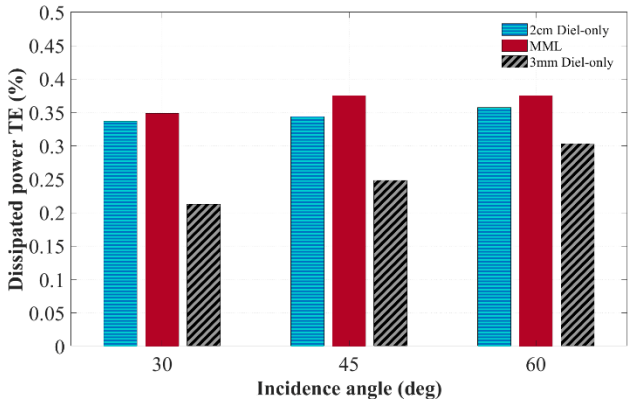

FIGURE 25. Dissipated power in the muscle tissue for a TE plane wave impinging at three different incidence angles. The considered air gap thickness is 2 mm.

Finally, the oblique incidence and air gap conditions are considered together to confirm the positive trend of the MML with respect to the dielectric only solutions. More in detail, three different angles of incidence (i.e. (θ = 30°, 45°, 60°) of both a TE and TM plane waves have been considered in the case of a 2 mm air gap. The results are illustrated in Fig. 24 and Fig.25 for the TM and TE case, respectively.

It is interesting to notice that the MML provides the best results for both polarizations with a significant overall improvement with respect to the dielectric matching layer of the same thickness (almost 20% more power reaches the muscle tissue for a TM incidence at 60°) and comparable or slightly better performance (7% more for a TM incidence at 60°) with respect to the thicker solution.

VII. CONCLUSION

A metasurface matching layer was proposed to provide a low-profile effective means for allowing a more efficient penetration of the electromagnetic field inside the body, particularly in the muscle tissue. A single dielectric layer design was considered and the use of thin slabs was enforced to allow for improved ergonomics (*i.e.* wearability) for the user. The illustrated metasurface solution can be tailored for optimal performance starting from the analysis of the impedance of the body at the targeted frequency. The proposed approach can help in decreasing the total amount of transmitted power for establishing a link with an implanted device or for a medical diagnosis. The electromagnetic field distribution, which is not homogeneous in the region close to the metasurface, recovers the typical behavior observed in dielectric-only matching layer cases and thus it is not critical in view of connection with internal probes. For the first time, the analysis has been carried out also for an oblique plane wave incidence and with an air gap between the applied matching layer and the skin. We found that the MML is beneficial for both conditions. From our comparisons, we concluded that the MML solution improves the penetration of the electromagnetic field into the muscle layer.

REFERENCES

[1] H.-J. Kim, H. Hirayama, S. Kim, K. J. Han, R. Zhang, and J.-W. Choi, "Review of near-field wireless power and communication for biomedical applications," *IEEE Access*, vol. 5, pp. 21264–21285, 2017, doi: 10.1109/ACCESS.2017.2757267.

[2] S. J. Priyadarshini and D. J. Hemanth, "Investigation and reduction methods of specific absorption rate for biomedical applications: A survey," *Int. J. RF Microw. Comput.-Aided Eng.*, vol. 28, no. 3, Mar. 2018, Art. no. e21211, doi: 10.1002/mmce.21211.

[3] K. N. Paracha, S. K. Abdul Rahim, P. J. Soh, and M. Khalily, "Wearable antennas: A review of materials, structures, and innovative features for autonomous communication and sensing," *IEEE Access*, vol. 7, pp. 56694–56712, 2019, doi: 10.1109/ACCESS.2019.2909146.

[4] M. I. Kitra, C. J. Panagamuwa, P. McEvoy, J. C. Vardaxoglou, and J. R. James, "Low SAR ferrite handset antenna design," *IEEE Trans. Antennas Propag.*, vol. 55, no. 4, pp. 1155–1164, Apr. 2007, doi: 10.1109/TAP.2007.893370.

[5] Z. H. Jiang and D. H. Werner, "A compact, wideband circularly polarized co-designed filtering antenna and its application for wearable devices with low SAR," *IEEE Trans. Antennas Propag.*, vol. 63, no. 9, pp. 3808–3818, Sep. 2015, doi: 10.1109/TAP.2015.2452942.

[6] O. Lauer, P. Frei, M.-C. Gosselin, W. Joseph, M. Röösli, and J. Fröhlich, "Combining near- and far-field exposure for an organ-specific and whole-body RF-EMF proxy for epidemiological research: A reference case," *Bioelectromagnetics*, vol. 34, no. 5, pp. 366–374, Jul. 2013, doi: 10.1002/bem.21782.

[7] A. Hirata, S. Kodera, J. Wang, and O. Fujiwara, "Dominant factors influencing whole-body average SAR due to far-field exposure in whole-body resonance frequency and GHz regions," *Bioelectromagnetics*, vol. 28, no. 6, pp. 484–487, Sep. 2007, doi: 10.1002/bem.20335.

[8] ICNIRP, "Guidelines for limiting exposure to time-varying electric, magnetic and electromagnetic fields (0 Hz to 300 GHz)," *Health Phys.*, vol. 74, no. 4, pp. 494–522, 1998.

[9] O. P. Gandhi, G. Lazzi, and C. M. Furse, "Electromagnetic absorption in the human head and neck for mobile telephones at 835 and 1900 MHz," *IEEE Trans. Microw. Theory Techn.*, vol. 44, no. 10, pp. 1884–1897, Oct. 1996, doi: 10.1109/22.539947.

[10] R. Takei, T. Nagaoka, K. Saito, S. Watanabe, and M. Takahashi, "SAR variation due to exposure from a smartphone held at various positions near the torso," *IEEE Trans. Electromagn. Compat.*, vol. 59, no. 2, pp. 747–753, Apr. 2017, doi: 10.1109/TEMC.2016.2642201.

[11] M. Klemm, I. J. Craddock, J. A. Leendertz, A. Preece, and R. Benjamin, "Radar-based breast cancer detection using a hemispherical antenna array—Experimental results," *IEEE Trans. Antennas Propag.*, vol. 57, no. 6, pp. 1692–1704, Jun. 2009, doi: 10.1109/TAP.2009.2019856.

[12] X. Li, M. Jalilvand, Y. L. Sit, and T. Zwick, "A compact double-layer on-body matched bowtie antenna for medical diagnosis," *IEEE Trans. Antennas Propag.*, vol. 62, no. 4, pp. 1808–1816, Apr. 2014, doi: 10.1109/TAP.2013.2297158.

[13] M. M. Paulides, J. F. Bakker, N. Chavannes, and G. C. Van Rhoon, "A patch antenna design for application in a phased-array head and neck hyperthermia applicator," *IEEE Trans. Biomed. Eng.*, vol. 54, no. 11, pp. 2057–2063, Nov. 2007, doi: 10.1109/TBME.2007.895111.

[14] P. T. Nguyen, A. Abbosh, and S. Crozier, "Microwave hyperthermia for breast cancer treatment using electromagnetic and thermal focusing tested on realistic breast models and antenna arrays," *IEEE Trans. Antennas Propag.*, vol. 63, no. 10, pp. 4426–4434, Oct. 2015, doi: 10.1109/TAP.2015.2463681.

[15] P. Momenroodaki, W. Haines, M. Fromandi, and Z. Popovic, "Noninvasive internal body temperature tracking with near-field microwave radiometry," *IEEE Trans. Microw. Theory Techn.*, vol. 66, no. 5, pp. 2535–2545, May 2018, doi: 10.1109/TMTT.2017.2776952.

[16] I. Butterworth, J. Seralles, C. S. Mendoza, L. Giancardo, and L. Daniel, "A wearable physiological hydration monitoring wristband through multi-path non-contact dielectric spectroscopy in the microwave range," in *IEEE MTT-S Int. Microw. Symp. Dig.*, Sep. 2015, pp. 60–61, doi: 10.1109/IMWS-BIO.2015.7303776.

[17] P. J. Soh, G. A. E. Vandenbosch, M. Mercuri, and D. M. M.-P. Schreurs, "Wearable wireless health monitoring: Current developments, challenges, and future trends," *IEEE Microw. Mag.*, vol. 16, no. 4, pp. 55–70, May 2015, doi: 10.1109/MMM.2015.2394021.

[18] A. Kiourti and K. S. Nikita, "Miniature scalp-implantable antennas for telemetry in the MICS and ISM bands: Design, safety considerations and link budget analysis," *IEEE Trans. Antennas Propag.*, vol. 60, no. 8, pp. 3568–3575, Aug. 2012, doi: 10.1109/TAP.2012.2201078.

[19] A. Kiourti and K. S. Nikita, "A review of in-body biotelemetry devices: Implantables, ingestibles, and injectables," *IEEE Trans. Biomed. Eng.*, vol. 64, no. 7, pp. 1422–1430, Jul. 2017, doi: 10.1109/TBME.2017.2668612.

[20] C. Liu, Y.-X. Guo, H. Sun, and S. Xiao, "Design and safety considerations of an implantable rectenna for far-field wireless power transfer," *IEEE Trans. Antennas Propag.*, vol. 62, no. 11, pp. 5798–5806, Nov. 2014, doi: 10.1109/TAP.2014.2352363.

[21] M. K. Magill, G. Conway, and W. Scanlon, "Tissue-independent implantable antenna for in-body communications at 2.36–2.5 GHz," *IEEE Trans. Antennas Propag.*, vol. 65, no. 9, pp. 4406–4417, Sep. 2017, doi: 10.1109/TAP.2017.2708119.

[22] P. W. Barber, O. P. Gandhi, M. J. Hagmann, and I. Chatterjee, "Electromagnetic absorption in a multilayered model of man," *IEEE Trans. Biomed. Eng.*, vol. BME-26, no. 7, pp. 400–405, Jul. 1979, doi: 10.1109/TBME.1979.326418.

[23] A. Christ, A. Klingenbock, T. Samaras, C. Goiceanu, and N. Kuster, "The dependence of electromagnetic far-field absorption on body tissue composition in the frequency range from 300 MHz to 6 GHz," *IEEE Trans. Microw. Theory Techn.*, vol. 54, no. 5, pp. 2188–2195, May 2006, doi: 10.1109/TMTT.2006.872789.

[24] S. M. Asif, A. Iftikhar, B. D. Braaten, D. L. Ewert, and K. Maile, "A wide-band tissue numerical model for deeply implantable antennas for RF-powered leadless pacemakers," *IEEE Access*, vol. 7, pp. 31031–31042, 2019, doi: 10.1109/ACCESS.2019.2902981.

[25] M. Fujii, R. Fujii, R. Yotsuki, T. Wuren, T. Takai, and I. Sakagami, "Exploration of whole human body and UWB radiation interaction by efficient and accurate two-debye-pole tissue models," *IEEE Trans. Antennas Propag.*, vol. 58, no. 2, pp. 515–524, Feb. 2010, doi: 10.1109/TAP.2009.2024968.

[26] R. Chavez-Santiago, A. Khaleghi, and I. Balasingham, "Matching layer for path loss reduction in ultra wideband implant communications," in *Proc. 36th Annu. Int. Conf. IEEE Eng. Med. Biol. Soc.*, Aug. 2014, pp. 6989–6992, doi: 10.1109/EMBC.2014.6945236.

[27] K. T. Karathanasis, I. A. Gouzouasis, I. S. Karanasiou, M. I. Giamalaki, G. Stratakos, and N. K. Uzunoglu, "Noninvasive focused monitoring and irradiation of head tissue phantoms at microwave frequencies," *IEEE Trans. Inf. Technol. Biomed.*, vol. 14, no. 3, pp. 657–663, May 2010, doi: 10.1109/TITB.2010.2040749.

[28] E. C. Fear, X. Li, S. C. Hagness, and M. A. Stuchly, "Confocal microwave imaging for breast cancer detection: Localization of tumors in three dimensions," *IEEE Trans. Biomed. Eng.*, vol. 49, no. 8, pp. 812–822, Aug. 2002, doi: 10.1109/TBME.2002.800759.

[29] W. C. Choi, S. Lim, and Y. J. Yoon, "Design of noninvasive hyperthermia system using transmit-array lens antenna configuration," *IEEE Antennas Wireless Propag. Lett.*, vol. 15, pp. 857–860, 2016, doi: 10.1109/LAWP.2015.2477428.

[30] S. Curto, P. McEvoy, X. Bao, and M. J. Ammann, "Compact patch antenna for electromagnetic interaction with human tissue at 434 MHz," *IEEE Trans. Antennas Propag.*, vol. 57, no. 9, pp. 2564–2571, Sep. 2009, doi: 10.1109/TAP.2009.2027040.

[31] J. Blauert and A. Kiourti, "Bio-matched horn: A novel 1–9 GHz on-body antenna for low-loss biomedical telemetry with implants," *IEEE Trans. Antennas Propag.*, vol. 67, no. 8, pp. 5054–5062, Aug. 2019, doi: 10.1109/TAP.2018.2889159.

[32] Y. Okano, S. Ogino, and K. Ishikawa, "Development of optically transparent ultrathin microwave absorber for ultrahigh-frequency RF identification system," *IEEE Trans. Microw. Theory Techn.*, vol. 60, no. 8, pp. 2456–2464, Aug. 2012, doi: 10.1109/TMTT.2012.2202680.

[33] X. Luo, M. Pu, X. Ma, and X. Li, "Taming the electromagnetic boundaries via metasurfaces: From theory and fabrication to functional devices," *Int. J. Antennas Propag.*, vol. 2015, pp. 1–80, 2015, doi: 10.1155/2015/204127.

[34] M. Zhang, W. Zhang, A. Q. Liu, F. C. Li, and C. F. Lan, "Tunable polarization conversion and rotation based on a reconfigurable metasurface," *Sci. Rep.*, vol. 7, no. 1, p. 12068, Dec. 2017.

[35] S. Genovesi, F. Costa, F. Fanciulli, and A. Monorchio, "Wearable inkjet-printed wideband antenna by using miniaturized AMC for sub-GHz applications," *IEEE Antennas Wireless Propag. Lett.*, vol. 15, pp. 1927–1930, 2016, doi: 10.1109/LAWP.2015.2513962.

[36] S. Zhu and R. Langley, "Dual-band wearable textile antenna on an EBG substrate," *IEEE Trans. Antennas Propag.*, vol. 57, no. 4, pp. 926–935, Apr. 2009, doi: 10.1109/TAP.2009.2014527.

[37] C. P. Scarborough, D. H. Werner, and D. E. Wolfe, "Compact low-profile tunable metasurface-enabled antenna with near-arbitrary polarization," *IEEE Trans. Antennas Propag.*, vol. 64, no. 7, pp. 2775–2783, Jul. 2016, doi: 10.1109/TAP.2016.2562666.

[38] G. Bianconi, F. Costa, S. Genovesi, and A. Monorchio, "Optimal design of dipole antennas backed by a finite high-impedance screen," *Prog. Electromagn. Res. C*, vol. 18, pp. 137–151, 2011, doi: 10.2528/PIERC10111204.

[39] D. Bianchi, S. Genovesi, M. Borgese, F. Costa, and A. Monorchio, "Element-independent design of wide-angle impedance matching radomes by using the generalized scattering matrix approach," *IEEE Trans. Antennas Propag.*, vol. 66, no. 9, pp. 4708–4718, Sep. 2018, doi: 10.1109/TAP.2018.2845449.

[40] T. R. Cameron and G. V. Eleftheriades, "Analysis and characterization of a wide-angle impedance matching metasurface for dipole phased arrays," *IEEE Trans. Antennas Propag.*, vol. 63, no. 9, pp. 3928–3938, Sep. 2015, doi: 10.1109/TAP.2015.2448231.

[41] R. E. Collin, *Field Theory of Guided Waves*. Hoboken, NJ, USA: Wiley, 1991.

[42] E. Groumpas, M. Koutsoupidou, I. S. Karanasiou, C. Papageorgiou, and N. Uzunoglu, "Real-time passive brain monitoring system using near-field microwave radiometry," *IEEE Trans. Biomed. Eng.*, vol. 67, no. 1, pp. 158–165, Jan. 2020.

[43] J. S. Ho, S. Kim, and A. S. Y. Poon, "Midfield wireless powering for implantable systems," *Proc. IEEE*, vol. 101, no. 6, pp. 1369–1378, Jun. 2013, doi: 10.1109/JPROC.2013.2251851.

[44] R. Mittra, C. H. Chan, and T. Cwik, "Techniques for analyzing frequency selective surfaces–A review," *Proc. IEEE*, vol. 76, no. 12, pp. 1593–1615, Dec. 1988, doi: 10.1109/5.16352.

[45] F. Costa, S. Genovesi, A. Monorchio, and G. Manara, "A circuit-based model for the interpretation of perfect metamaterial absorbers," *IEEE Trans. Antennas Propag.*, vol. 61, no. 3, pp. 1201–1209, Mar. 2013, doi: 10.1109/TAP.2012.2227923.

[46] *Ansys HFSS*. Accessed: Nov. 30, 2020. [Online] https://www.ansys.com/products/electronics/ansys-hfss

[47] M. Borgese, F. A. Dicandia, F. Costa, S. Genovesi, and G. Manara, "An inkjet printed chipless RFID sensor for wireless humidity monitoring," *IEEE Sensors J.*, vol. 17, no. 15, pp. 4699–4707, Aug. 2017, doi: 10.1109/JSEN.2017.2712190.

[48] C. A. Balanis, *Advanced Engineering Electromagnetics*, 2nd ed. Hoboken, NJ, USA: Wiley.

SIMONE GENOVESI (Senior Member, IEEE) received the Laurea degree in telecommunication engineering and the Ph.D. degree in information engineering from the University of Pisa, Pisa, Italy, in 2003 and 2007, respectively. Since 2003, he has been collaborating with the Electromagnetic Communication Laboratory, Pennsylvania State University (Penn State), University Park. From 2004 to 2006, he was a Research Associate with the ISTI Institute, National Research Council of Italy (ISTI-CNR), Pisa. From 2015 to 2017, he was a short-term Visiting Researcher at the Grenoble Institute of Technology, Valence, France, and University Rovira I Virgili, Tarragona, Spain, for several times. He is currently an Associate Professor with the Dipartimento di Ingegneria dell'Informazione, University of Pisa. He is also the Coordinator of the Additive Manufacturing founded in the framework of the Departments of Excellence (Dipartimenti di Eccellenza) funded by the Italian Ministry of Education, University and Research. His current research interests include radio frequency identification (RFID) systems, reconfigurable antennas, and metameterials.

IAN RICHARD BUTTERWORTH (Member, IEEE) received the B.Eng. degree in electronic engineering from the University of Warwick, U.K., and the M.Sc. degree in audio acoustics from the University of Salford, U.K. In 2008, he joined the National Physical Laboratory, U.K., as a Research Scientist, where he undertook research covering acousto-optic measurement of acoustic and ultrasonic fields, quantification of ultrasonic cavitation, and thermal safety monitoring in medical ultrasound devices. In 2013, he joined the Massachusetts Institute of Technology, USA, as a Biomedical Research Fellow, working on translational research projects, including the development of sensors for monitoring of physiological hydration state, a device for non-invasive screening for low-white blood cell count, and the monitoring of free computer typing for assessing Parkinsons disease progression.

JOSÉ ENRIQUE CRUZ SERRALLÉS (Graduate Student Member, IEEE) is currently pursuing the Ph.D. degree with the Computational Prototyping Group, Electrical Engineering and Computer Science Department, MIT. He is currently a Research Assistant with the Computational Prototyping Group, Electrical Engineering and Computer Science Department, MIT. His research interests include inverse problems (specifically in MRI), optimization-guided design (such as coil design), adjoint methods for optimization, and computational electromagnetics. He received the ISMRM Magna Cum Laude Merit Award in 2017 and the Lemelson Engineering Presidential Fellowship Award in 2017.

LUCA DANIEL (Senior Member, IEEE) is currently a Professor of electrical engineering and computer science with MIT. His research interest includes development of numerical techniques (i.e., uncertainty quantification, inverse problems, robust optimization, parameterized model order reduction, and integral equation solvers) for large complex systems (e.g., magnetic resonance imaging scanners, power networks, silicon photonics, and deep neural networks). He has received Best Paper Awards from several journals of the IEEE, such as IEEE TRANSACTIONS ON POWER ELECTRONICS, IEEE TRANSACTIONS ON COMPUTER AIDED DESIGN, and IEEE TRANSACTIONS ON COMPONENTS, PACKAGING, AND MANUFACTURING. He has also received 13 Best-Paper Awards at international conferences, such as the IEEE Early Career Award, the IBM Corporation Faculty Award, the Spira Award for Excellence in Teaching from the MIT School of Engineering, and the Best Ph.D. Thesis Awards from the Mathematics and the Electrical Engineering Departments, UC Berkeley, and the Association in Computing Machinery (ACM).